First double-differential cross section measurement of neutral-current π^0 production in neutrino-argon scattering in the MicroBooNE detector

P. Abratenko,[38] O. Alterkait,[38] D. Andrade Aldana,[15] L. Arellano,[21] J. Asaadi,[37] A. Ashkenazi,[35] S. Balasubramanian,[12] B. Baller,[12] A. Barnard,[28] G. Barr,[28] D. Barrow,[28] J. Barrow,[25] V. Basque,[12] J. Bateman,[21] O. Benevides Rodrigues,[15] S. Berkman,[24] A. Bhanderi,[21] A. Bhat,[7] M. Bhattacharya,[12] M. Bishai,[3] A. Blake,[18] B. Bogart,[23] T. Bolton,[17] J. Y. Book,[14] M. B. Brunetti,[41] L. Camilleri,[10] Y. Cao,[21] D. Caratelli,[4] F. Cavanna,[12] G. Cerati,[12] A. Chappell,[41] Y. Chen,[31] J. M. Conrad,[22] M. Convery,[31] L. Cooper-Troendle,[29] J. I. Crespo-Anadón,[6] R. Cross,[41] M. Del Tutto,[12] S. R. Dennis,[5] P. Detje,[5] R. Diurba,[2] Z. Djurcic,[1] R. Dorrill,[15] K. Duffy,[28] S. Dytman,[29] B. Eberly,[33] P. Englezos,[30] A. Ereditato,[7,12] J. J. Evans,[21] R. Fine,[19] W. Foreman,[15] B. T. Fleming,[7] D. Franco,[7] A. P. Furmanski,[25] F. Gao,[4] D. Garcia-Gamez,[13] S. Gardiner,[12] G. Ge,[10] S. Gollapinni,[19] E. Gramellini,[21] P. Green,[28] H. Greenlee,[12] L. Gu,[18] W. Gu,[3] R. Guenette,[21] P. Guzowski,[21] L. Hagaman,[7] M. Handley,[5] O. Hen,[22] C. Hilgenberg,[25] G. A. Horton-Smith,[17] Z. Imani,[38] B. Irwin,[25] M. S. Ismail,[29] C. James,[12] X. Ji,[26] J. H. Jo,[3] R. A. Johnson,[8] Y.-J. Jwa,[10] D. Kalra,[10] N. Kamp,[22] G. Karagiorgi,[10] W. Ketchum,[12] M. Kirby,[3] T. Kobilarcik,[12] I. Kreslo,[2] N. Lane,[21] I. Lepetic,[30] J.-Y. Li,[11] Y. Li,[3] K. Lin,[30] B. R. Littlejohn,[15] H. Liu,[3] W. C. Louis,[19] X. Luo,[4] C. Mariani,[40] D. Marsden,[21] J. Marshall,[41] N. Martinez,[17] D. A. Martinez Caicedo,[32] S. Martynenko,[3] A. Mastbaum,[30] I. Mawby,[18] N. McConkey,[39] V. Meddage,[17] J. Mendez,[20] J. Micallef,[22,38] K. Miller,[7] A. Mogan,[9] T. Mohayai,[16] M. Mooney,[9] A. F. Moor,[5] C. D. Moore,[12] L. Mora Lepin,[21] M. M. Moudgalya,[21] S. Mulleriababu,[2] D. Naples,[29] A. Navrer-Agasson,[21] N. Nayak,[3] M. Nebot-Guinot,[11] J. Nowak,[18] N. Oza,[10] O. Palamara,[12] N. Pallat,[25] V. Paolone,[29] A. Papadopoulou,[1] V. Papavassiliou,[27] H. B. Parkinson,[11] S. F. Pate,[27] N. Patel,[18] Z. Pavlovic,[12] E. Piasetzky,[35] K. Pletcher,[24] I. Pophale,[18] X. Qian,[3] J. L. Raaf,[12] V. Radeka,[3] A. Rafique,[1] M. Reggiani-Guzzo,[11,21] L. Ren,[27] L. Rochester,[31] J. Rodriguez Rondon,[32] M. Rosenberg,[38] M. Ross-Lonergan,[19] I. Safa,[10] G. Scanavini,[42] D. W. Schmitz,[7] A. Schukraft,[12] W. Seligman,[10] M. H. Shaevitz,[10] R. Sharankova,[12] J. Shi,[5] E. L. Snider,[12] M. Soderberg,[34] S. Söldner-Rembold,[21] J. Spitz,[23] M. Stancari,[12] J. St. John,[12] T. Strauss,[12] A. M. Szelc,[11] W. Tang,[36] N. Taniuchi,[5] K. Terao,[31] C. Thorpe,[21] D. Torbunov,[3] D. Totani,[4] M. Toups,[12] A. Trettin,[21] Y.-T. Tsai,[31] J. Tyler,[17] M. A. Uchida,[5] T. Usher,[31] B. Viren,[3] J. Wang,[26] M. Weber,[2] H. Wei,[20] A. J. White,[7] S. Wolbers,[12] T. Wongjirad,[38] M. Wospakrik,[12] K. Wresilo,[5] W. Wu,[29] E. Yandel,[4] T. Yang,[12] L. E. Yates,[12] H. W. Yu,[3] G. P. Zeller,[12] J. Zennamo,[12] and C. Zhang[3]

(The MicroBooNE Collaboration)*

[1] *Argonne National Laboratory (ANL), Lemont, IL, 60439, USA*
[2] *Universität Bern, Bern CH-3012, Switzerland*
[3] *Brookhaven National Laboratory (BNL), Upton, NY, 11973, USA*
[4] *University of California, Santa Barbara, CA, 93106, USA*
[5] *University of Cambridge, Cambridge CB3 0HE, United Kingdom*
[6] *Centro de Investigaciones Energéticas, Medioambientales y Tecnológicas (CIEMAT), Madrid E-28040, Spain*
[7] *University of Chicago, Chicago, IL, 60637, USA*
[8] *University of Cincinnati, Cincinnati, OH, 45221, USA*
[9] *Colorado State University, Fort Collins, CO, 80523, USA*
[10] *Columbia University, New York, NY, 10027, USA*
[11] *University of Edinburgh, Edinburgh EH9 3FD, United Kingdom*
[12] *Fermi National Accelerator Laboratory (FNAL), Batavia, IL 60510, USA*
[13] *Universidad de Granada, Granada E-18071, Spain*
[14] *Harvard University, Cambridge, MA 02138, USA*
[15] *Illinois Institute of Technology (IIT), Chicago, IL 60616, USA*
[16] *Indiana University, Bloomington, IN 47405, USA*
[17] *Kansas State University (KSU), Manhattan, KS, 66506, USA*
[18] *Lancaster University, Lancaster LA1 4YW, United Kingdom*
[19] *Los Alamos National Laboratory (LANL), Los Alamos, NM, 87545, USA*
[20] *Louisiana State University, Baton Rouge, LA, 70803, USA*
[21] *The University of Manchester, Manchester M13 9PL, United Kingdom*
[22] *Massachusetts Institute of Technology (MIT), Cambridge, MA, 02139, USA*
[23] *University of Michigan, Ann Arbor, MI, 48109, USA*
[24] *Michigan State University, East Lansing, MI 48824, USA*
[25] *University of Minnesota, Minneapolis, MN, 55455, USA*
[26] *Nankai University, Nankai District, Tianjin 300071, China*

[27] New Mexico State University (NMSU), Las Cruces, NM, 88003, USA
[28] University of Oxford, Oxford OX1 3RH, United Kingdom
[29] University of Pittsburgh, Pittsburgh, PA, 15260, USA
[30] Rutgers University, Piscataway, NJ, 08854, USA
[31] SLAC National Accelerator Laboratory, Menlo Park, CA, 94025, USA
[32] South Dakota School of Mines and Technology (SDSMT), Rapid City, SD, 57701, USA
[33] University of Southern Maine, Portland, ME, 04104, USA
[34] Syracuse University, Syracuse, NY, 13244, USA
[35] Tel Aviv University, Tel Aviv, Israel, 69978
[36] University of Tennessee, Knoxville, TN, 37996, USA
[37] University of Texas, Arlington, TX, 76019, USA
[38] Tufts University, Medford, MA, 02155, USA
[39] University College London, London WC1E 6BT, United Kingdom
[40] Center for Neutrino Physics, Virginia Tech, Blacksburg, VA, 24061, USA
[41] University of Warwick, Coventry CV4 7AL, United Kingdom
[42] Wright Laboratory, Department of Physics, Yale University, New Haven, CT, 06520, USA

We report the first double-differential cross section measurement of neutral-current neutral pion (NCπ^0) production in neutrino-argon scattering, as well as single-differential measurements of the same channel in terms of final states with and without protons. The kinematic variables of interest for these measurements are the π^0 momentum and the π^0 scattering angle with respect to the neutrino beam. A total of 4971 candidate NCπ^0 events fully-contained within the MicroBooNE detector are selected using data collected at a mean neutrino energy of ~ 0.8 GeV from 6.4×10^{20} protons on target from the Booster Neutrino Beam at the Fermi National Accelerator Laboratory. After extensive data-driven model validation to ensure unbiased unfolding, the Wiener-SVD method is used to extract nominal flux-averaged cross sections. The results are compared to predictions from commonly used neutrino event generators, which tend to overpredict the measured NCπ^0 cross section, especially in the 0.2-0.5 GeV/c π^0 momentum range, at forward scattering angles, and when at least one proton is present in the final state. These measurements show sensitivity to a variety of features that complicate the description of NCπ^0 production including the form factors describing the elementary neutrino interaction and the final state interactions of the outgoing particles in the residual argon nucleus. This data will help improve the modeling of NCπ^0 production, which represents a major background in measurements of charge-parity violation in the neutrino sector and in searches for new physics beyond the Standard Model.

Modern accelerator-based neutrino experiments are capable of expansive physics programs that address a variety of important topics. These include charge-parity violation in the neutrino sector [1, 2], the neutrino mass ordering [3], measurements of rare Standard Model processes [4–7], searches for sterile neutrinos [8, 9] and other physics beyond the standard model (BSM) [10, 11]. Many of these analyses require measuring the rate of interactions that produce single electrons [12–16], single photons [4, 6], or boosted and overlapping e^+e^- or $\gamma\gamma$ pairs [17–20] by selecting events that leave an electromagnetic shower signature in the detector. In the few-GeV neutrino energy regime relevant to these experiments, neutral-current neutral pion (NCπ^0) production represents the primary background in single-shower selections.

Below neutrino energies of about 1.5 GeV, the NCπ^0 channel is dominated by resonance interactions [21–24] where the initial neutrino-nucleon scattering produces a $\Delta(1232)$ baryon that can decay to a nucleon and a π^0 that exit the nucleus. Coherent scattering [25], where the neutrino interacts with the nucleus as a whole rather than an individual nucleon, and final state interactions (FSI) experienced by hadrons produced through other interaction modes [26, 27] also contribute to π^0 production. These processes are sub-dominant yet important in a robust description of the NCπ^0 channel.

Outside the nucleus, the π^0 decays to two photons with a 99% branching ratio, resulting in a two shower topology. If one of these photons is not reconstructed, the NCπ^0 event will be misidentified as a single-shower event leading to their prominence in single-shower selections. Precise theoretical modeling of NCπ^0 production is thus needed to maximize the physics reach of neutrino experiments. This requires the support of detailed measurements of NCπ^0 production, which are sparse [28–30], especially on argon and in the few-GeV regime.

To this end, we report the first double-differential cross section measurement of NCπ^0 production in neutrino-argon scattering. The kinematics of the final state neutral pions are quantified by performing the measurement as a function of the π^0 momentum, P_{π^0}, and the cosine of the π^0 scattering angle with respect to the neutrino beam, $\cos\theta_{\pi^0}$. The signal definition includes events in which a neutrino of any flavor scatters via the neutral-current process and produces a single final state π^0 with $P_{\pi^0} < 1.2$ GeV/c. The upper limit on the momentum

* microboone_info@fnal.gov

restricts the measurement to regions of phase space with appreciable signal. Any hadronic final state not including an additional π^0 is included in the signal definition.

In the same variables, single-differential measurements in terms of final states with and without protons are also reported. These use the signal definition outlined above but divide the semi-inclusive channel ("Xp") into final states containing no protons with kinetic energy above 35 MeV ("0p") and final states containing at least one proton with kinetic energy above 35 MeV ("Np"). Understanding the 0p and Np final states is particularly important for experiments employing liquid argon time projection chambers (LArTPCs) [31–35], which may utilize the presence of a gap between the neutrino and shower vertices to help differentiate electrons from photons [36–39]. The tendency for no additional neutrino vertex activity in single-shower 0p events makes this topology particularly challenging and increases the NCπ^0 background in these selections. This is especially important when testing BSM models, many of which predict single-shower final states without hadronic activity [17–20].

This work utilizes the data set collected with the MicroBooNE LArTPC detector [40] and 6.4×10^{20} protons on target (POT) from the Booster Neutrino Beam (BNB) [41]. The BNB is primarily composed of ν_μ (93.7%) with smaller $\bar{\nu}_\mu$ (5.8%) and $\nu_e/\bar{\nu}_e$ (0.5%) components. The MicroBooNE detector's TPC has 85 tonnes of liquid argon active mass and an array of 32 photomultiplier tubes (PMTs). Interactions that produce charged particles in the TPC create scintillation light and ionization electrons. The light is recorded by the PMTs which provides ns-scale timing for interactions [42]. The ionization electrons drift in a 273 V/cm electric field and induce charge on a set of three wire readout planes. Individual wire charge distributions are deconvolved from the detector response [43–45] and serve as inputs to the Wire-Cell topographical three-dimensional image processing algorithm [46]. This event reconstruction chain provides the basis for particle identification, calorimetry, and event selection [47].

The Wire-Cell reconstruction identifies particle candidates by finding kinks in a cluster of activity in-time with the neutrino beam [47]. Track and electromagnetic shower topologies are separated based on the amount of large-angle scattering, the proximity to additional isolated activity, and the width of the activity perpendicular to its trajectory. Candidate neutrino interaction vertices are formed concurrently alongside the hypothesized final state particles and their decay and scattering products based on the rate of deposited charge (dQ/dx), topology of the final state, and particle relationships [47]. A final neutrino vertex is chosen by a `SparseConvNet` neural network [48].

A shower's energy is reconstructed from its total deposited charge multiplied by a scale factor obtained from simulation that accounts for bias in charge reconstruction and the average recombination effect [49–51]. An additional 0.95 scaling factor is applied to data based on previous π^0 mass calibration; this factor is not applied to the simulation [37]. The energy of tracks longer than 4 cm that stop within the active volume of the detector is calculated based on range using the NIST PSTAR database [52] with a correction for different particle masses. For all other tracks, the kinetic energy is calculated by converting their dQ/dx to dE/dx with an effective recombination model [47, 53].

Neutral pions are reconstructed based on the identification of the two photons and their associated topological information. For events with more than two showers, the pair with the highest energy is used. The distance between the neutrino vertex and π^0 vertex is used to separate primary pions from those produced in reinteractions outside the target nucleus. When NC events do not have additional hadronic activity to identify the π^0 vertex, the point on the each shower's primary axis that is closest to the opposite shower's primary axis is identified. The midpoint of the line connecting these two points is labeled as the displaced π^0 vertex and the direction of each shower is redefined with respect to that vertex [47].

Monte Carlo (MC) simulations are used to train the boosted decision tree (BDT) event selection and estimate inputs to the data unfolding. The neutrino flux model utilizes MiniBooNE's `Geant4`-based simulation of the BNB [41, 54]. Neutrino-argon interactions are simulated with the `G18_10a_02_11a` configuration of the `GENIE v3.0.6` event generator [55, 56] that has been tuned to CC0π data from T2K [57, 58]. The tune has little impact on these measurements because it only affects charged-current (CC) quasi-elastic and meson-exchange-current events. Final state particles are propagated through a model of the detector using the `Geant4` toolkit `v4_10_3_03c` [54] and `LArSoft` [59] framework. The simulated TPC and PMT waveforms are overlaid on data taken without the neutrino beam to provide an accurate description of the cosmic ray backgrounds. These overlaid MC samples are processed with the Wire-Cell reconstruction in the same manner as real data.

The first step in selecting NCπ^0 events is rejecting through-going and stopping cosmic ray muons with algorithms that match TPC-charge to PMT-light [49, 60]. This forms the basis of the "generic neutrino selection" which reduces cosmic backgrounds to about 15% without imposing requirements on the nature of the neutrinos participating in the interactions. A BDT was then trained using the `XGBoost` library [61] on variables previously used to identify CC events [37] as well as additional reconstructed parameters designed to identify NCπ^0 events. The training uses a signal enhanced sample of 40k events with the final BDT cut chosen based on maximising the product of the efficiency and purity. The selection achieves an efficiency of 35% as estimated by the `GENIE`-based MicroBooNE MC. A total of 4971

candidate events fully-contained (FC) within the detector are selected when the BDT is applied to the data. This selection is estimated to have a 54% purity for signal events. Figures illustrating the reconstruction quality, event selection efficiency, and measured distributions are presented in the Supplemental Material.

For the measurements of final states with and without protons, the selection is split into 0p and Np samples based on the presence of a reconstructed proton with kinetic energy greater than 35 MeV. This yields 1452 FC candidate Np NCπ^0 data events and 3519 FC candidate 0p NCπ^0 data events. The threshold is motivated by MicroBooNE's ability to detect tracks > 1 cm in length, which corresponds to 35 MeV for protons, and is the energy at which the proton detection efficiency approaches 50% [62]. Of the NCπ^0 signal events passing the Np (0p) selection, 92% (54%) are estimated to satisfy the Np (0p) signal criteria.

The reconstructed π^0 momentum, $P^{rec}_{\pi^0}$, and cosine of the reconstructed π^0 scattering angle, $\cos\theta^{rec}_{\pi^0}$, are calculated using the showers produced by the two photons associated with the π^0 decay. The opening angle of the showers, $\theta_{\gamma\gamma}$, and the energy of each shower, E_{γ_1} and E_{γ_2}, is used to reconstruct $P^{rec}_{\pi^0}$ according to

$$P^{rec}_{\pi^0} = m_{\pi^0}\sqrt{\frac{2}{(1-\alpha^2)(1-\cos\theta_{\gamma\gamma})}-1}, \qquad (1)$$

where $m_{\pi^0} = 0.135$ GeV/c^2 is the π^0 mass [63], and $\alpha = (E_{\gamma_1} - E_{\gamma_2})/(E_{\gamma_1} + E_{\gamma_2})$. The $P^{rec}_{\pi^0}$ resolution ranges from about 15% at low momenta to about 40% at high momenta. The π^0 scattering angle is calculated from the momentum of the two showers, P_{γ_1} and P_{γ_2}, according to

$$\cos\theta^{rec}_{\pi^0} = \frac{P^z_{\gamma_1} + P^z_{\gamma_2}}{\sqrt{(P^x_{\gamma_1} + P^x_{\gamma_2})^2 + (P^y_{\gamma_1} + P^y_{\gamma_2})^2 + (P^z_{\gamma_1} + P^z_{\gamma_2})^2}}. \qquad (2)$$

The absolute $\cos\theta^{rec}_{\pi^0}$ resolution is around 0.1 but degrades at backwards angles for the 0p selection.

Systematic uncertainties on the reconstructed distributions are estimated with a total covariance matrix, $V^{\rm sys} = V_{\rm flux} + V_{\rm reint} + V_{\rm xs} + V_{\rm det} + V^{\rm stat}_{\rm MC} + V_{\rm dirt} + V_{\rm POT} + V_{\rm Target}$, obtained by summing the covariance matrices calculated for each source of uncertainty. The uncertainties on the BNB flux [41] are contained in $V_{\rm flux}$, and the neutrino-argon interaction modeling uncertainties [58] are accounted for in $V_{\rm xs}$. These both contribute (5-15)% uncertainty to the extracted cross sections and are similar in size to the data statistical uncertainty, except in some low count bins where the statistical uncertainty grows to (30-40)%. Uncertainties on reinteractions outside the target nucleus are accounted for in $V_{\rm reint}$ using `Geant4Reweight` [64]. These have little impact on the extracted results. The multi-sim technique [65] is used to calculate $V_{\rm flux}$, $V_{\rm xs}$, and $V_{\rm reint}$. Detector response uncertainties [66] are accounted for in $V_{\rm det}$ with a uni-sim approach. As in [37, 67], a single parameter is altered by 1σ and bootstrapping [68] is used to estimate the impact of this variation. Detector effects are the largest source of uncertainty on these measurements, usually contributing at the (10-25)% level though rising to (30-60)% at high P_{π^0} and backwards $\cos\theta_{\pi^0}$. This is largely driven by significant detector uncertainties on the background prediction partially due to there being a lower number of background MC events available for bootstrapping. Also included are flat 50%, 2% and 1% uncertainties on neutrino interactions outside the detector ($V_{\rm dirt}$), POT counting ($V_{\rm POT}$), and the number of target nuclei ($V_{\rm Target}$), respectively. Their impact on the total uncertainty is small. The Supplemental Material contains figures illustrating the contribution of each source of uncertainty to the total uncertainty on the extracted results.

Wiener-SVD unfolding [69] is used to extract nominal flux-averaged cross section results [70]. The inputs for this method are the measurement M, the response matrix R that describes the mapping between the true and reconstructed distributions predicted by the MC, and the reconstructed space covariance matrix $V = V^{\rm sys} + V^{\rm stat}$, where $V^{\rm stat}$ contains the data statistical uncertainty obtained following the combined Neyman-Pearson procedure [71]. The unfolding returns a regularized cross section and corresponding covariance matrix, V_S. An additional smearing matrix, A_C, capturing the bias induced by regularization is also obtained in the unfolding [69]. Any prediction should be multiplied by A_C when making a comparison to the data result. The extracted cross sections, A_C, and V_S can be found in the Supplemental Material.

The 0p and Np cross sections are extracted simultaneously following the formalism outlined in [62], which accounts for the correlations between the 0p and Np channels during unfolding. This allows the number of true Np events in the 0p selection to be predicted based on the observation of the Np selection (and vice versa), thereby minimizing the overall dependence on the model. Alongside the FC sample, a smaller sample of 1467 events partially-contained (PC) within the detector are also collected and used in the unfolding. Due to larger uncertainties and lower event counts, these distributions have minimal impact on the results. Blockwise unfolding [62, 72] is also employed to obtain inter-variable correlations for the unfolded results.

Model inaccuracies can bias cross section measurements through inadequate estimations of the selection efficiency, background prediction, and the mapping between true and reconstructed variables. Data-driven model validation is employed to verify that the model, including its uncertainties, is sufficient for the unfolding. The model is deemed adequate if it can describe the data at the 2σ level. This is quantified with χ^2 goodness-of-fit tests between measured and predicted distributions

interpreted by using the number of degrees of freedom, ndf, which corresponds to the number of bins, to obtain p-values. To better expose relevant mismodeling, these tests utilize the conditional constraint formalism [73]. The conditional constraint leverages correlations between different channels and variables to update the model prediction and reduce the uncertainties on one distribution based on data observations in another distribution. The cross section extraction does not utilize these constraints, which are used strictly for model validation. This data-driven methodology is analogous to the model validation in other MicroBooNE analyses [37, 62, 67, 74, 75]. The model validation tests described in further detail below can be found in the Supplemental Material.

Validating the modeling of π^0 kinematics starts by constraining the FC $P_{\pi^0}^{rec}$ prediction with the reconstructed neutrino energy distribution of the ν_μCC selection from [37, 62]. This constraint reduces correlated flux and detector uncertainties shared between NCπ^0 and ν_μCC events thereby better exposing the cross section modeling. This test is conducted on the distributions for the 0p, Np and Xp channels to evaluate each hadronic final state. Good agreement is observed, with p-values of 0.94, 0.84, and 0.80, for 0p, Np and Xp distributions, respectively. The same test is performed individually on all four angular slices used for the double-differential measurement and on the total reconstructed energy rather than P_{π^0}. The MC is able to describe the data within uncertainties in these tests with p-values close to one in all cases.

To evaluate the modeling of the π^0 kinematics further, the FC $P_{\pi^0}^{rec}$ distribution is used to constrain the FC $\cos\theta_{\pi^0}^{rec}$ prediction. Correlations in the statistical uncertainties, arising from the fact that the constraining and constrained distributions utilize the same events, are estimated using a bootstrapping procedure [62, 68]. These tests are applied to each hadronic final state and indicate that the data is described with uncertainties with p-values close to one in all cases. Alongside the tests on the $P_{\pi^0}^{rec}$ and reconstructed energy distributions in angular slices, this demonstrates that the overall model is sufficient for the extraction of the double-differential cross section as a function of $\cos\theta_{\pi^0}$ and P_{π^0}.

The modeling of the proton kinematics is important for the simultaneous measurement of the 0p and Np NCπ^0 cross sections. As such, the proton kinematics are evaluated with two separate constraints on the FC leading proton kinetic energy distribution. First, the reconstructed neutrino energy distribution from the ν_μCC channel [37, 62] is used; this results in a p-value of 0.90. Second, the FC π^0 kinematics are used; this constraint results in a p-value of 0.94. Together, with the validation of the P_{π^0}, $\cos\theta_{\pi^0}$, and reconstructed energy distributions for both the 0p and Np channels, these tests indicate that the model is sufficient for the simultaneous extraction of the 0p and Np cross sections.

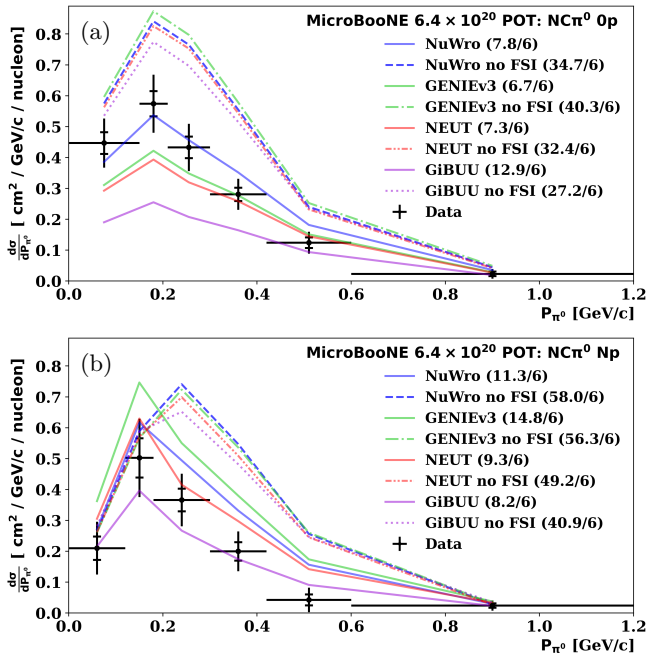

FIG. 1: Unfolded 0p (a) and Np (b) P_{π^0} differential cross sections. The black inner (outer) error bars on the data points represent the statistical (total) uncertainties on the extracted cross section corresponding to the square root of the diagonal elements of the extracted covariance matrix. Generator predictions are indicated by the colored lines with corresponding χ^2/ndf values displayed in the legend.

All aforementioned model validation tests are also applied to the PC distributions. These all yield p-values close to one.

The extracted cross section results are compared to event generator predictions from `GENIE v3.0.6 G18_10a_02_11a` (`GENIEv3`) [55], `NuWro 21.02` (`NuWro`) [76], `GiBUU 2023` (`GiBUU`) [77], and `NEUT 5.4.0.1` (`NEUT`) [78]. To demonstrate the utility of these measurements, these comparisons include predictions which modify the FSI experienced by the outgoing particles, or the form factors describing the neutrino-nucleon interaction. Generator predictions were processed with the `NUISANCE` framework [79], do not include theoretical uncertainties, and are smeared with the A_C obtained from unfolding. Agreement with the data is quantified by χ^2 values calculated with uncertainties according to V_S.

The simultaneously extracted 0p and Np P_{π^0} differential cross sections are shown in Fig. 1 alongside generator predictions with and without FSI. Compared to the "no FSI" predictions, the predictions with FSI reduce the cross section, shift the peak of the P_{π^0} distribution towards lower values resulting in a sharper drop just beyond the peak, and are favored by the data. This is unsurprising as similar features are well established in measurements of photoproduction of pions on nuclear targets [80] where, despite involving different probes, the FSI are identical to neutrino scattering. Neverthe-

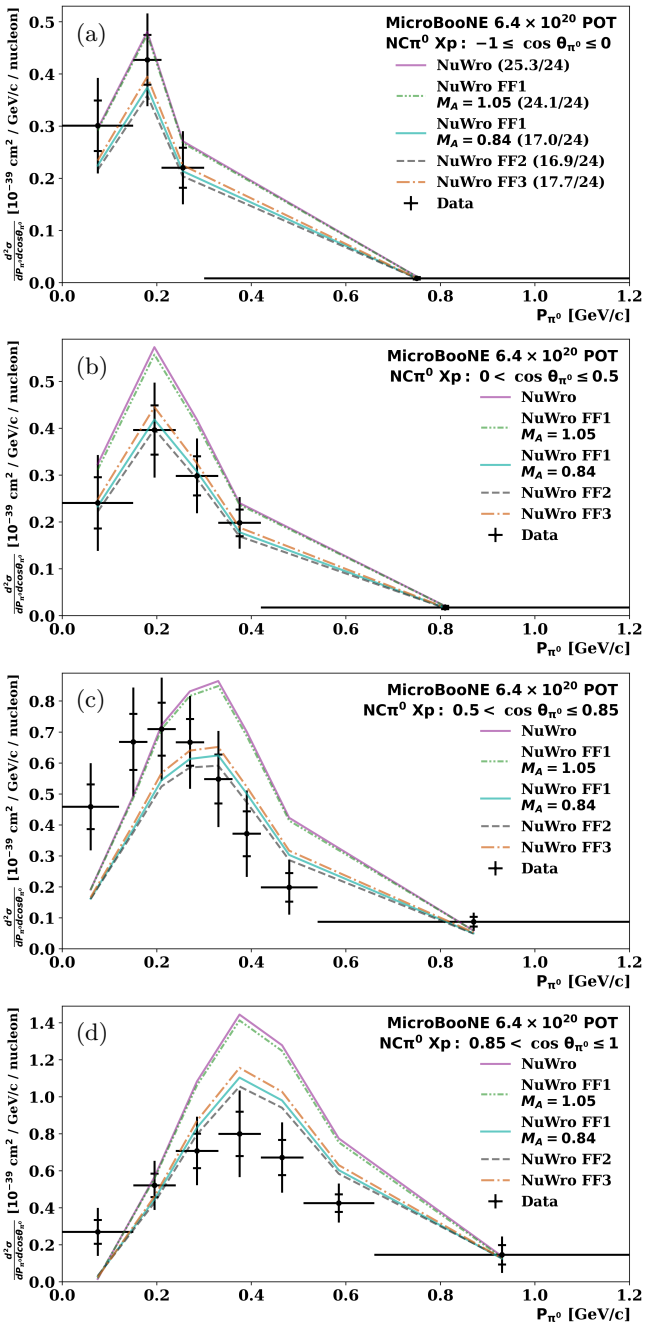

FIG. 2: Same as Fig. 1, but for the $\cos\theta_{\pi^0}$ and P_{π^0} double-differential Xp cross section result. Predictions from `NuWro` using various parameterizations of the neutrino-nucleon Δ excitation cross section are shown. Each subfigure shows a different $\cos\theta_{\pi^0}$ angular region, with the χ^2/ndf calculated across all bins displayed in the legend of (a).

less, the predictions with FSI still overestimate the measured Np NCπ^0 cross section, particularly around the 0.2-0.5 GeV/c momentum range. The exception to this is `GiBUU`, which instead underestimates the cross section around the peak of the distribution in both the 0p and Np channels. This observation is interesting given that `GiBUU` shows a better description of other MicroBooNE 0p measurements on the ν_μCC channel [62, 74] than other generators do. Its low normalisation here points towards important subtleties in the treatment of FSI between nucleons, resonances, and mesons [81]. The 0.2-0.5 GeV/c momentum range is strongly impacted by FSI, suggesting that refinements to FSI modeling may enable a better description of this data.

Figure 2 shows the unfolded double-differential Xp cross section result as a function of P_{π^0} for specific $\cos\theta_{\pi^0}$ regions. `NuWro` predictions with various parameterizations of the $C_5^A(Q^2)$ axial form factor [82, 83] used to describe the neutrino-nucleon Δ excitation cross section are also shown. Free parameters of these form factors are fit to ANL [84, 85] and BNL [86] CCπ^+ bubble chamber data. Though demonstrated to be consistent within flux uncertainties [82, 87], these data sets differ in normalization by approximately 30% leading to large theoretical uncertainties. The default `NuWro` prediction uses a dipole form factor with an axial mass, M_A, of 0.94 GeV/c^2 as obtained in [82] with a fit to both the ANL and BNL data. The predictions labeled `NuWro FF1 MA=1.05` and `NuWro FF1 MA=0.84` use the modified dipole form factor given in Eq. (II.12) of [83] with $M_A = 1.05$ GeV/c^2 and $M_A = 0.84$ GeV/c^2, respectively. Two additional predictions with steeper Q^2 dependence for $C_5^A(Q^2)$ are also included. These are labeled `NuWro FF2` and `NuWro FF3` and correspond to the form factors in [83] with steeper Q^2 dependence and $M_A = 1.05$ GeV/c^2 and $M_A = 0.95$ GeV/c^2, respectively.

The default `NuWro` dipole prediction and modified dipole prediction with $M_A = 1.05$ GeV/c^2 tend to overestimate the measured NCπ^0 cross section. Better agreement is seen when M_A is reduced to 0.84 GeV/c^2 or when the steeper Q^2 dependence is introduced. This is illustrated in Fig. 2, which shows that the `NuWro FF1 MA=0.84`, `NuWro FF2` and `NuWro FF3` predictions agree better with the data than `NuWro` and `NuWro FF1 MA=1.05`. In [82], the dipole prediction analogous to `NuWro` also overestimates the ANL data. Similarly, in [83], the prediction utilizing the same form factors as `NuWro FF1` overestimates the ANL bubble chamber data with $M_A = 1.05$ GeV/c^2 and better agreement is obtained with $M_A = 0.84$ GeV/c^2 and with the steeper Q^2 dependence. These observations are consistent with what is seen in Fig. 2 and indicate that predictions agreeing better with the ANL data may also be favored by this NCπ^0 data.

In addition to the measurements described above, simultaneously extracted 0p and Np $\cos\theta_{\pi^0}$ differential cross sections are presented in the Supplemental Material. Semi-inclusive Xp single-differential cross sections in P_{π^0} and $\cos\theta_{\pi^0}$ are also included.

In summary, we report the first double-differential cross section measurements of neutral-current π^0 production in neutrino-argon scattering. Single-differential measurements in terms of final states with and without protons are also reported. These measurements are per-

formed with a boosted decision tree based event selection and, after extensive model validation to ensure unbiased unfolding, are extracted with the Wiener-SVD method. Commonly used neutrino event generators overestimate the measured NCπ^0 cross section, especially for π^0 momentum around 0.2-0.5 GeV/c, at forward scattering angles, and when a proton is present in the final state. The exception to this is `GiBUU`, which instead underestimates the cross section. The unfolded results show sensitivity to the form factors describing the elementary neutrino interaction and the modeling of final state interactions.

This document was prepared by the MicroBooNE collaboration using the resources of the Fermi National Accelerator Laboratory (Fermilab), a U.S. Department of Energy, Office of Science, HEP User Facility. Fermilab is managed by Fermi Research Alliance, LLC (FRA), acting under Contract No. DE-AC02-07CH11359. MicroBooNE is supported by the following: the U.S. Department of Energy, Office of Science, Offices of High Energy Physics and Nuclear Physics; the U.S. National Science Foundation; the Swiss National Science Foundation; the Science and Technology Facilities Council (STFC), part of the United Kingdom Research and Innovation; the Royal Society (United Kingdom); and the UK Research and Innovation (UKRI) Future Leaders Fellowship. Additional support for the laser calibration system and cosmic ray tagger was provided by the Albert Einstein Center for Fundamental Physics, Bern, Switzerland. We also acknowledge the contributions of technical and scientific staff to the design, construction, and operation of the MicroBooNE detector as well as the contributions of past collaborators to the development of MicroBooNE analyses, without whom this work would not have been possible.

[1] K. Abe *et al.* (T2K Collaboration), Constraint on the matter–antimatter symmetry-violating phase in neutrino oscillations, Nature **580**, 339 (2020).

[2] C. Hagedorn *et al.*, CP violation in the lepton sector and implications for leptogenesis, Int. J. Mod. Phys. A **33**, 1842006 (2018).

[3] X. Qian and P. Vogel, Neutrino Mass Hierarchy, Prog. Part. Nucl. Phys. **83**, 1 (2015), arXiv:1505.01891 [hep-ex].

[4] P. Abratenko *et al.* (MicroBooNE Collaboration), Search for Neutrino-Induced Neutral-Current Δ Radiative Decay in MicroBooNE and a First Test of the MiniBooNE Low Energy Excess under a Single-Photon Hypothesis, Phys. Rev. Lett. **128**, 111801 (2022).

[5] C. Kullenberg *et al.* (NOMAD Collaboration), A search for single photon events in neutrino interactions, Phys. Lett. B **706**, 268 (2012).

[6] K. Abe *et al.* (T2K Collaboration), Search for neutral-current induced single photon production at the ND280 near detector in T2K, J. Phys. G **46**, 08LT01 (2019).

[7] P. Abratenko *et al.* (MicroBooNE Collaboration), First measurement of η meson production in neutrino interactions on argon with MicroBooNE, Phys. Rev. Lett. **132**, 151801 (2024), arXiv:2305.16249 [hep-ex].

[8] M. A. Acero *et al.*, White Paper on Light Sterile Neutrino Searches and Related Phenomenology (2023), Snowmass report, arXiv:2203.07323 [hep-ex].

[9] C. Giunti and T. Lasserre, eV-Scale Sterile Neutrinos, Annu. Rev. Nucl. Part. Sci. **69**, 163 (2019).

[10] B. Batell *et al.*, Dark Sector Studies with Neutrino Beams (2022), Contribution to Snowmass 2021, arXiv:2207.06898 [hep-ph].

[11] C. A. Argüelles *et al.*, New opportunities at the next-generation neutrino experiments I: BSM neutrino physics and dark matter, Rep. Prog. Phys. **83**, 124201 (2020).

[12] P. Abratenko *et al.* (MicroBooNE Collaboration), First constraints on light sterile neutrino oscillations from combined appearance and disappearance searches with the MicroBooNE detector, Phys. Rev. Lett. **130**, 011801 (2023).

[13] A. A. Aguilar-Arevalo *et al.* (MiniBooNE Collaboration), Updated MiniBooNE neutrino oscillation results with increased data and new background studies, Phys. Rev. D **103**, 052002 (2021).

[14] K. Abe *et al.* (T2K Collaboration), Improved constraints on neutrino mixing from the T2K experiment with 3.13×10^{21} protons on target, Phys. Rev. D **103**, 112008 (2021).

[15] M. A. Acero *et al.* (The NOνA Collaboration), Improved measurement of neutrino oscillation parameters by the NOνA experiment, Phys. Rev. D **106**, 032004 (2022).

[16] P. Adamson and others. (MINOS+ Collaboration), Precision Constraints for Three-Flavor Neutrino Oscillations from the Full MINOS+ and MINOS Dataset, Phys. Rev. Lett. **125**, 131802 (2020).

[17] P. Abratenko *et al.* (MicroBooNE collaboration), First search for dark-trident processes using the MicroBooNE detector (2023), arXiv:2312.13945 [hep-ex].

[18] W. Abdallah, R. Gandhi, and S. Roy, Two-Higgs doublet solution to the LSND, MiniBooNE and muon $g-2$ anomalies, Phys. Rev. D **104**, 055028 (2021).

[19] A. M. Abdullahi *et al.*, A panorama of new-physics explanations to the MiniBooNE excess (2023), arXiv:2308.02543 [hep-ph].

[20] C. Cesarotti *et al.*, New μ Forces From ν_μ Sources (2023), arXiv:2311.10829 [hep-ph].

[21] D. Rein and L. M. Sehgal, Neutrino-excitation of baryon resonances and single pion production, Ann. Phys. **133**, 79 (1981).

[22] G. Fogli and G. Nardulli, Neutral current induced one-pion production: A new model and its comparison with experiment, Nucl. Phys. B **165**, 162 (1980).

[23] T. Leitner, O. Buss, U. Mosel, and L. Alvarez-Ruso, Neutrino-induced pion production at energies relevant for the MiniBooNE and K2K experiments, Phys. Rev. C **79**, 038501 (2009).

[24] O. Lalakulich, E. A. Paschos, and G. Piranishvili, Resonance production by neutrinos: The second resonance region, Phys. Rev. D **74**, 014009 (2006).

[25] D. Rein and L. M. Sehgal, Coherent π^0 production in neutrino reactions, Nucl. Phys. B **223**, 29 (1983).

[26] T. Leitner, L. Alvarez-Ruso, and U. Mosel, Neutral cur-

rent neutrino-nucleus interactions at intermediate energies, Phys. Rev. C **74**, 065502 (2006).
[27] O. Lalakulich and U. Mosel, Comparison of GiBUU calculations with MiniBooNE pion production data (2013), Proceedings of the NuInt12 Workshop, arXiv:1304.2409 [nucl-th].
[28] A. A. Aguilar-Arevalo *et al.* (MiniBooNE Collaboration), Measurement of ν_μ and $\overline{\nu}_\mu$ induced neutral current single π^0 production cross sections on mineral oil at $E_\nu \sim \mathcal{O}$ (1 GeV), Phys. Rev. D **81**, 013005 (2010).
[29] P. Abratenko *et al.* (MicroBooNE Collaboration), Measurement of neutral current single π^0 production on argon with the MicroBooNE detector, Phys. Rev. D **107**, 012004 (2023).
[30] R. Acciarri *et al.* (ArgoNeuT Collaboration), Measurement of ν_μ and $\overline{\nu}_\mu$ neutral current $\pi^0 \to \gamma\gamma$ production in the ArgoNeuT detector, Phys. Rev. D **96**, 012006 (2017).
[31] C. Rubbia, *The liquid-argon time projection chamber: a new concept for neutrino detectors*, Tech. Rep. CERN-EP-INT-77-8 (1977).
[32] H. H. Chen *et al.*, *A Neutrino detector sensitive to rare processes. I. A Study of neutrino electron reactions*, Tech. Rep. FERMILAB-PROPOSAL-0496 (1976).
[33] W. Willis and V. Radeka, Liquid-argon ionization chambers as total-absorption detectors, Nucl. Instrum. Meth. A **120**, 221 (1974).
[34] D. R. Nygren, *The Time Projection Chamber: A New 4 π Detector for Charged Particles*, Tech. Rep. PEP-0144 (SLAC, 1974).
[35] F. Cavanna, A. Ereditato, and B. T. Fleming, Advances in liquid argon detectors, Nucl. Instrum. Meth. A **907**, 1 (2018).
[36] P. Abratenko *et al.* (MicroBooNE Collaboration), Search for an anomalous excess of charged-current ν_e interactions without pions in the final state with the MicroBooNE experiment, Phys. Rev. D **105**, 112004 (2022).
[37] P. Abratenko *et al.* (MicroBooNE Collaboration), Search for an anomalous excess of inclusive charged-current ν_e interactions in the MicroBooNE experiment using Wire-Cell reconstruction, Phys. Rev. D **105**, 112005 (2022).
[38] P. Abratenko *et al.* (MicroBooNE Collaboration), Search for an anomalous excess of charged-current quasielastic ν_e interactions with the MicroBooNE experiment using Deep-Learning-based reconstruction, Phys. Rev. D **105**, 112003 (2022).
[39] P. Abratenko *et al.* (MicroBooNE Collaboration), Search for an excess of electron neutrino interactions in MicroBooNE using multiple final-state topologies, Phys. Rev. Lett. **128**, 241801 (2022).
[40] R. Acciarri *et al.* (MicroBooNE Collaboration), Design and construction of the MicroBooNE detector, J. Instrum. **12** (02), P02017.
[41] A. A. Aguilar-Arevalo *et al.* (MiniBooNE Collaboration), Neutrino flux prediction at MiniBooNE, Phys. Rev. D **79**, 072002 (2009).
[42] P. Abratenko *et al.* (MicroBooNE Collaboration), First demonstration of $\mathcal{O}$(1 ns) timing resolution in the MicroBooNE liquid argon time projection chamber, Phys. Rev. D **108**, 052010 (2023).
[43] R. Acciarri *et al.* (MicroBooNE Collaboration), Noise Characterization and Filtering in the MicroBooNE Liquid Argon TPC, J. Instrum. **12** (08), P08003, arXiv:1705.07341 [physics.ins-det].
[44] C. Adams *et al.* (MicroBooNE Collaboration), Ionization electron signal processing in single phase LArTPCs. Part I. Algorithm Description and quantitative evaluation with MicroBooNE simulation, J. Instrum. **13** (07), P07006, arXiv:1802.08709 [physics.ins-det].
[45] C. Adams *et al.* (MicroBooNE Collaboration), Ionization electron signal processing in single phase LArTPCs. Part II. Data/simulation comparison and performance in MicroBooNE, J. Instrum. **13** (07), P07007, arXiv:1804.02583 [physics.ins-det].
[46] X. Qian *et al.*, Three-dimensional Imaging for Large LArTPCs, J. Instrum. **13** (05), P05032, arXiv:1803.04850 [physics.ins-det].
[47] P. Abratenko *et al.* (MicroBooNE Collaboration), Wire-cell 3D pattern recognition techniques for neutrino event reconstruction in large LArTPCs: algorithm description and quantitative evaluation with MicroBooNE simulation, J. Instrum. **17** (01), P01037.
[48] B. Graham, M. Engelcke, and L. van der Maaten, 3D Semantic Segmentation with Submanifold Sparse Convolutional Networks, in *2018 IEEE/CVF Conference on Computer Vision and Pattern Recognition* (2018) pp. 9224–9232.
[49] P. Abratenko *et al.* (MicroBooNE Collaboration), Neutrino event selection in the MicroBooNE liquid argon time projection chamber using Wire-Cell 3D imaging, clustering, and charge-light matching, J. Instrum. **16** (06), P06043.
[50] E. Shibamura *et al.*, Drift velocities of electrons, saturation characteristics of ionization and W-values for conversion electrons in liquid argon, liquid argon-gas mixtures and liquid xenon, Nucl. Instrum. Methods Phys. Res. **131**, 249 (1975).
[51] M. Miyajima *et al.*, Average energy expended per ion pair in liquid argon, Phys. Rev. A **9**, 1438 (1974).
[52] PSTAR at NIST: `https://physics.nist.gov/PhysRefData/Star/Text/PSTAR.html`.
[53] C. Adams *et al.* (MicroBooNE Collaboration), Calibration of the charge and energy loss per unit length of the MicroBooNE liquid argon time projection chamber using muons and protons, J. Instrum. **15** (03), P03022.
[54] S. Agostinelli *et al.*, Geant4—a simulation toolkit, Nucl. Instrum. Meth. A **506**, 250 (2003).
[55] L. Alvarez-Ruso *et al.* (GENIE Collaboration), Recent highlights from GENIE v3, Eur. Phys. J. ST **230**, 4449 (2021).
[56] C. Andreopoulos *et al.*, The GENIE Neutrino Monte Carlo Generator, Nucl. Instrum. Meth. A **614**, 87 (2010), arXiv:0905.2517 [hep-ph].
[57] K. Abe *et al.* (T2K Collaboration), Measurement of double-differential muon neutrino charged-current interactions on C_8H_8 without pions in the final state using the T2K off-axis beam, Phys. Rev. D **93**, 112012 (2016).
[58] P. Abratenko *et al.* (MicroBooNE Collaboration), New CC0π GENIE model tune for MicroBooNE, Phys. Rev. D **105**, 072001 (2022).
[59] E. Snider and G. Petrillo, LArSoft: toolkit for simulation, reconstruction and analysis of liquid argon TPC neutrino detectors, J. Phys. Conf. Ser **898**, 042057 (2017).
[60] P. Abratenko *et al.* (MicroBooNE Collaboration), Cosmic Ray Background Rejection with Wire-Cell LArTPC Event Reconstruction in the MicroBooNE Detector, Phys. Rev. Appl. **15**, 064071 (2021).
[61] T. Chen and C. Guestrin, XGBoost: A Scalable Tree Boosting System, in *Proceedings of the 22nd ACM*

SIGKDD International Conference on Knowledge Discovery and Data Mining (2016) p. 785–794.
[62] P. Abratenko *et al.* (MicroBooNE Collaboration), Inclusive cross section measurements in final states with and without protons for charged-current ν_μ-Ar scattering in MicroBooNE, arXiv preprint (2024), arXiv:2402.19216 [hep-ex].
[63] C. Patrignani *et al.* (Particle Data Group), Review of Particle Physics, Chin. Phys. **C40**, 100001 (2016).
[64] J. Calcutt, C. Thorpe, K. Mahn, and L. Fields, Geant4Reweight: a framework for evaluating and propagating hadronic interaction uncertainties in Geant4, J. Instrum. **16** (08), P08042.
[65] B. P. Roe, Statistical errors in Monte Carlo estimates of systematic errors, Nucl. Instrum. Meth. A **570**, 159 (2007).
[66] P. Abratenko *et al.* (MicroBooNE Collaboration), Novel approach for evaluating detector-related uncertainties in a LArTPC using MicroBooNE data, Eur. Phys. J. C **82**, 454 (2022).
[67] P. Abratenko *et al.* (MicroBooNE Collaboration), First Measurement of Energy-Dependent Inclusive Muon Neutrino Charged-Current Cross Sections on Argon with the MicroBooNE Detector, Phys. Rev. Lett. **128**, 151801 (2022).
[68] M. R. Chernick *et al.*, *International Encyclopedia of Statistical Science* (Springer Berlin Heidelberg, Berlin, Heidelberg, 2011) pp. 169–174.
[69] W. Tang *et al.*, Data Unfolding with Wiener-SVD Method, J. Instrum. **12** (10), P10002, arXiv:1705.03568 [physics.data-an].
[70] L. Koch and S. Dolan, Treatment of flux shape uncertainties in unfolded, flux-averaged neutrino cross-section measurements, Phys. Rev. D **102**, 113012 (2020).
[71] X. Ji, W. Gu, X. Qian, H. Wei, and C. Zhang, Combined Neyman–Pearson chi-square: An improved approximation to the Poisson-likelihood chi-square, Nucl. Instrum. Meth. A **961**, 163677 (2020).
[72] S. Gardiner, Mathematical methods for neutrino cross-section extraction, arXiv preprint (2024), FERMILAB-PUB-23-692-CSAID, arXiv:2401.04065 [hep-ex].
[73] M. L. Eaton, *Multivariate Statistics: a Vector Space Approach* (John Wiley and Sons, 1983) pp. 116–117.
[74] P. Abratenko *et al.* (MicroBooNE Collaboration), First simultaneous measurement of differential muon-neutrino charged-current cross sections on argon for final states with and without protons using MicroBooNE data, arXiv preprint (2024), arXiv:2402.19281 [hep-ex].
[75] P. Abratenko *et al.* (MicroBooNE Collaboration), Measurement of triple-differential inclusive muon-neutrino charged-current cross section on argon with the MicroBooNE detector (2023), arXiv:2307.06413 [hep-ex].
[76] T. Golan, J. Sobczyk, and J. Żmuda, NuWro: the Wrocław Monte Carlo Generator of Neutrino Interactions, Nucl. Phys. B Proc. Suppl. **229-232**, 499 (2012).
[77] O. Buss *et al.*, Transport-theoretical description of nuclear reactions, Phys. Rep. **512**, 1 (2012).
[78] Y. Hayato and L. Pickering, The NEUT neutrino interaction simulation program library, Eur. Phys. J. ST **230**, 4469 (2021).
[79] P. Stowell *et al.*, NUISANCE: a neutrino cross-section generator tuning and comparison framework, J. Instrum. **12** (01), P01016.
[80] B. Krusche *et al.*, Photoproduction of π mesons from nuclei, Eur. Phys. J. A **22**, 277–291 (2004).
[81] S. Dytman *et al.*, Comparison of validation methods of simulations for final state interactions in hadron production experiments, Phys. Rev. D **104**, 053006 (2021), arXiv:2103.07535 [hep-ph].
[82] K. M. Graczyk, D. Kiełczewska, P. Przewłocki, and J. T. Sobczyk, C_5^A axial form factor from bubble chamber experiments, Phys. Rev. D **80**, 093001 (2009).
[83] O. Lalakulich and E. A. Paschos, Resonance production by neutrinos: $J = 3/2$ resonances, Phys. Rev. D **71**, 074003 (2005).
[84] S. J. Barish *et al.*, Study of neutrino interactions in hydrogen and deuterium. II. Inelastic charged-current reactions, Phys. Rev. D **19**, 2521 (1979).
[85] G. M. Radecky *et al.*, Study of single-pion production by weak charged currents in low-energy νd interactions, Phys. Rev. D **25**, 1161 (1982).
[86] T. Kitagaki *et al.*, Study of $\nu d \to \mu^- pp_s$ and $\nu d \to \mu^- \Delta^{++}(1232) n_s$ using the BNL 7-foot deuterium-filled bubble chamber, Phys. Rev. D **42**, 1331 (1990).
[87] C. Wilkinson *et al.*, Reanalysis of bubble chamber measurements of muon-neutrino induced single pion production, Phys. Rev. D **90**, 112017 (2014).